Contributions of a Long Side Chain to the Binding Affinity of an Anthracene Derivative to DNA

Naga K. Modukuru, Kimberly J. Snow, Bradley S. Perrin, Jr., Jyotsna Thota, and Challa V. Kumar*

Department of Chemistry, University of Connecticut, Storrs, Connecticut 06269-3060

Received: February 25, 2005; In Final Form: April 16, 2005

Systematic studies on the DNA binding of a new anthracene derivative, carrying a 1,8-octyldiamine side chain, were carried out. Calorimetric, spectroscopic, and helix melting studies show that the side chain, consisting of eight methylene groups, enhances the binding constant by a factor of ∼35 when compared to the binding of a probe lacking the long side chain. Furthermore, the enthalpy of binding of the long-chain derivative to calf thymus DNA ($\Delta H = 4.1 \pm 0.1$ kcal/mol) is far greater than the sum of the enthalpy changes associated with the binding of the probe lacking the long side chain, and the enthalpy for the binding of 1,8-octyldiamine·2HCl. Strong synergistic effects, therefore, are seen with the long-chain derivative. Spectroscopic data indicate bathochromism, strong hypochromism, and quenching of anthryl fluorescence when the above ligand binds to calf thymus DNA. Fluorescence energy transfer studies and circular dichroism data strongly suggest intercalation of the anthryl ring system. The binding stabilizes the double helix, and the helix melting temperature is increased from 78 °C to >90 °C. The binding to DNA is reversible, depended on the ionic strength, and the major binding mode was suppressed at high ionic strengths and a new mode begins to dominate binding. Substitution of the anthracene ring with 1,8-octyldiamine chain provided a simple method to enhance the binding constant by nearly a factor of 35.

Introduction

Developing a clearer understanding of the interaction of small molecules with DNA is helpful in designing improved chemotherapeutic approaches.[1] Anthracene derivatives, in particular, received considerable attention as potential antitumor drugs. One of the anthracene derivatives tested in clinical trials was pseudourea and its analogues.[2,3,4] These derivatives bind tightly to DNA (Chart 1),[5,6] and they carry side chains or substituents that are protonated at physiological pH, which further strengthens the binding interaction.[5] Our long-term interest has been to probe the interactions of anthracene derivatives with DNA by systematically varying the substituents at the 9 and 10 positions of the anthracene ring system.

Anthracene derivatives are known to bind to DNA by several binding modes, and intercalation is one of the dominant binding modes.[7,8] For example, 9-anthrylmethylammonium chloride (AMAC, Chart 2) provided one of the first examples of the intercalation of the anthryl nucleus.[9] AMAC had no sequence preference for binding, but 9-anthrylpropylammonium chloride (APAC) prefers binding to AT rich regions over GC regions.[10,11] However, these small substituents did not influence the overall binding affinities. For example, AMAC, APAC, and N-Et-AMAC (Chart 2) indicated binding constants in the range of $\sim 1 \times 10^4$ M^{-1}.[9] This observation inspired us to test if a long hydrophobic side chain would enhance the binding affinity. Here, a simple method to enhance the overall binding affinity of the anthryl probes by more than an order of magnitude is presented.

Anthracene derivative of 1,8-octyldiamine (AODA), shown in Chart 2, carries a 11-atom side chain consisting of eight CH_2 groups, and two ammonium functions. The increased charge of AODA, when compared to AMAC, is expected to promote binding via electrostatic interactions. The long side chain is isostructural to the polyamine, spermidine, which is known to bind in the DNA minor groove.[12] This substituent at the 9-position is not expected to pose steric congestion for the intercalation

CHART 1: Major Modes for the Binding of Small Molecules to the DNA Double Helix

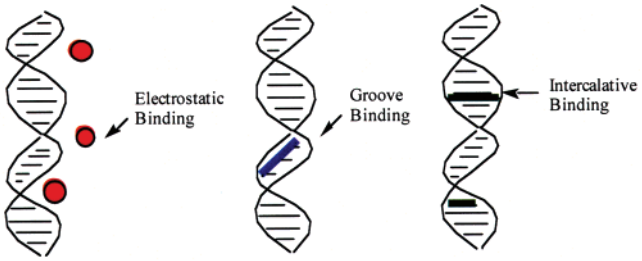

CHART 2: Structures of AMAC, APAC, N-Et-AMAC, and AODA

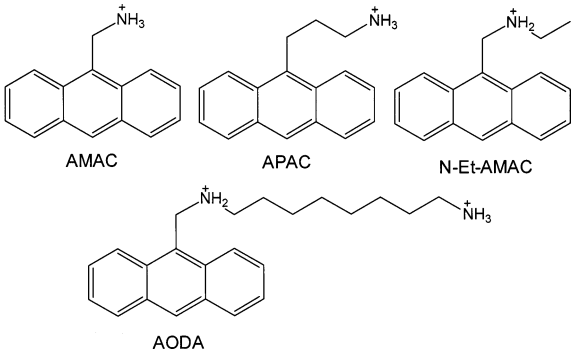

* To whom correspondence should be addressed. E-mail: Challa.Kumar@uconn.edu.

10.1021/jp050995d CCC: $30.25
Published on Web 05/19/2005

or groove binding. The hydrophobic regions of the side chain are expected to disfavor placing the side chain in the negatively charged DNA grooves, but its removal from the aqueous phase is expected to be entropically favorable. Therefore, it is intriguing to test if the long hydrophobic side chain of AODA would promote or disfavor binding to the DNA helix. A strong contribution of the octyl side chain of AODA to enhance it's binding to CTDNA is demonstrated here, by calorimetric and spectroscopic investigations.

Calorimetric data indicated that the enthalpy changes accompanying the binding of AODA to calf thymus DNA (CT DNA) are much greater than the sum of the enthalpy changes observed for the binding of AMAC and 1,8-octyldiamine·2HCl. A strong synergism between the side chain and the anthryl ring system is, therefore, noted.

Experimental Section

CT DNA (type I) was purchased from Sigma Chemical Co., and the sample was purified according to published protocols.[13] Stock solutions of DNA were prepared with Tris buffer (5 mM Tris, 50 mM NaCl, pH 7.2), and the concentration is expressed in terms of base pairs, unless mentioned otherwise. AMAC and APAC were synthesized as reported previously.[9]

Synthesis of AODA. AODA was synthesized by following a suitable modification of a published procedure, and the sample has been characterized by spectroscopic methods. A mixture of 9-chloromethylanthracene (300 mg, 1.3 mmol, 1 equiv), 10 equiv of K_2CO_3 (1.8244 g, 13.22 mmol), 0.3 equiv of KI (0.0657 g, 0.039 mmol), and 2 equiv of 1,8-diaminooctane (0.3810 g, 2.6 mmol) were mixed in acetonitrile (30 mL). The reaction mixture was refluxed for 6 h, and after cooling to room temperature, the inorganic solids were removed by filtration. The solvent was evaporated to produce a pale yellow product. The crude product was washed with hexane and diethyl ether (20 mL, three times each) to remove unreacted amine, and the residue has been crystallized from a mixture of methanol and toluene (1:1). The yield was 60% (mp: 185−86) UV−vis: 334, 350, 368, and 388 nm. Fluorescence: 394, 414, and 440 nm. ^{1}H NMR (ppm, multiplicity, and relative intensity): 8.78, singlet, 1; 8.38, doublet, 2; 8.35, doublet, 2; 7.73, triplet, 2; 7.72, triplet, 2; 5.18, singlet, 2; 3.46, multiplet, 2; 2.79, multiplet, 2; 1.69, multiplet, 2; 1.52, multiplet, 2; 1.15, multiplet, 10. Mass (*m*/*e*): M^+, 335.

Isothermal Titration Calorimetry. The binding constants with CT DNA were estimated by isothermal titration method using VP-ITC from MicroCal Inc., CT DNA (100 μM, 5 mM Tris, 50 mM NaCl, pH 7.2) solution was loaded into the calorimetric cell (1.4167 mL), while the reference cell contained water, and both cells have been thermally equilibrated at room temperature. AODA solution (558 μM AODA, 5 mM Tris, 50 mM NaCl, pH 7.2) was degassed under reduced pressure and loaded into the syringe, and predetermined volumes of the probe solutions were injected into the cell under constant stirring. The number of injections, the volume of each addition, and the time interval between successive injections were chosen using the software, and the whole process has been automated. Heat produced or absorbed due to each addition of the titrant was recorded and the corresponding thermograms have been obtained. The resulting data were analyzed using Origin software (v.5.0, Microcal Inc.) to estimate the binding constant, binding site size, enthalpy of binding, entropy of binding, and the free energy of binding. Each experiment was repeated multiple times, each data set was fitted several times with different initial estimates, and statistically reasonable data have been obtained.

The heat released or absorbed (Q) during the titration is related to the molar heat of ligand binding (ΔH), volume of the sample cell (V_o), the bulk concentration of the ligand (X_t), concentration of DNA (M_t), the intrinsic binding constant (K_b), and the number of binding sites (n) by the following eq 1:

$$Q = 0.5(nM_t\Delta HV_o)\,[1+(X_t/nM_t) + (1/nK_bM_t) - \sqrt{[(1 + (X_t/nM_t) + (1/nK_bM_t))^2 - 4X_t/nM_t]} ...] \quad (1)$$

The above equation was derived from basic thermodynamic principles, under equilibrium conditions, as described in the literature.[14]

Absorption Spectral Studies. Absorption spectra were recorded on SLM Aminco 3000 diode array spectrophotometer, which has been interfaced with an IBM personal computer. Concentrations of CTDNA solutions were determined by absorption spectroscopy ($\epsilon_{258\ nm} = 13\ 600\ M^{-1}\ cm^{-1}$).[15] Purity of the CTDNA was checked by monitoring the ratio of the absorbance at 260 nm to that at 280 nm. Absorption titrations with CTDNA were performed by keeping the concentration of the probe constant while increasing the concentration of CTDNA, and the data have been corrected for small increases in the volume (<10%).

Fluorescence Studies. Fluorescence spectra were recorded using an SLM 48000 spectrophotometer interfaced with an IBM personal computer. As in the case of the absorption titrations, a concentrated solution of CT DNA was added to the probe solution. The probe concentration was kept constant while increasing the DNA concentration, and the spectra have been corrected for volume changes. Probe/DNA mixtures were excited at their corresponding isosbestic points, wavelengths where the absorption is independent of DNA concentration, and the isosbestic points have been previously determined from the absorption titrations.

Binding Plots and Hypochromism. The spectral changes observed in the absorption measurements were used to calculate the intrinsic binding constant (K_b) by the Scatchard equation (2).[16] In eq 2, C_f is the concentration of the free probe, $r = C_b$/[DNA] where C_b is the concentration of the bound probe, and n is the binding site size. Concentration of the bound probe is given by $C_b = \Delta A/\Delta\epsilon$ where $\Delta A = A_f - A_b$ and $\Delta\epsilon = \epsilon_f - \epsilon_b$. A_f and A_b are the absorbances at the corresponding peak positions of the free and bound probes, respectively. The symbols ϵ_f and ϵ_b are the extinction coefficients of the free and bound probe, respectively. Half-reciprocal plots of absorbance vs 1/[DNA] were used to obtain ϵ_b, and the binding plots have been constructed from these data. The percent hypochromism was calculated as equal to $(\epsilon_f - \epsilon_b)/100$.

$$1/C_f = (K_bn/r) - K_b \quad (2)$$

Circular Dichroism (CD) Studies. The CD spectra were recorded on a JASCO J-710 spectropolarimeter interfaced with a Dell Optiplex personal computer, and the data have been acquired using software from JASCO. Solutions containing the probe and CT DNA were placed in a quartz cell (1 cm path length), and the spectra have been recorded in the 300−500 nm region. To reduce the interference from absorption by DNA, in the 200−300 nm region, a shorter path length cuvette (0.05 cm) was used for measurements in this region. The operating parameters of 1 nm bandwidth, sensitivity of10 millidegrees, and response time of 4 s were used to average upto16 scans for each sample.

Helix Melting Studies. Helix melting studies were carried out by a Cary Win 100 spectrophotometer equipped with a

thermostat under the control by a Dell Optiplex personal computer. Helix melting was monitored by following the absorbance of the sample at 280 nm or at 260 nm, as needed. The melting temperature (T_m) was determined from the first derivative of a plot of absorption vs T. Helix melting studies were carried out in Tris buffer (5 mM Tris, 25 mM NaCl, pH 7.2) using 25 μM AODA and 40 μM CT DNA.

Computational Modeling. Selected properties of AODA were calculated by using Computer Aided Chemistry (CAChe v.4.5) from Fujitsu, running on a Blue and White G3/G4 Apple Macintosh computer. Sequentially, the geometry of AODA was optimized and the frequencies of first harmonic virbational modes were calculated using the Molecular Orbital Package (MOPAC) and PM5 parameter set. Electronic absorption spectra were calculated using the ZINDO package, with the INDO/1 parameter set, after the geometry of AODA was optimized.

Results and Discussion

The thermodynamic and spectroscopic studies of the long chain derivative (AODA, Chart 2) show that the long side chain exerts a strong influence on the overall binding affinity. Both enthalpic and entropic contributions to the binding are noted, and these indicated a strong synergy between the side chain and the anthryl nucleus for binding to DNA. Spectroscopic data presented below are consistent with the intercalative binding of AODA with its side chain buried in the groove.

Calorimetric Studies. Calorimetric methods provide a direct method to estimate the thermodynamic parameters for the binding, and the heat produced during the binding of AODA to CT DNA was measured by ITC studies (Figure 1A). Each addition of a solution of AODA (558 μM) to the calorimeter cell, which contained a solution of CT DNA (100 μM), resulted in the release of heat until the binding is saturated. The time gap between the injections, the volume of the injectant, and the number of injections have been adjusted such that the binding is complete toward the end of the titration. In a separate experiment, the heat of dilution of AODA (upper curve, offset for clarity, Figure 1A), as well as the dilution of CT DNA (not shown), has been measured in a similar manner. The area under each peak was integrated, heats of dilution are subtracted, and the thermogram for the binding of AODA to CT DNA has been obtained (Figure 1B).

The net release of heat during the binding of AODA to CT DNA indicates that binding is exothermic, and that the binding saturates around 60 μM AODA. The heat released during the binding is related to the binding constant, the number of binding sites available, and thermodynamic parameters of the binding equilibrium.[17] Best fits to the data in Figure 1B required a one-site binding model, and these analyses resulted in the binding parameters $K_b = 4.0 \pm 0.4 \times 10^5\ M^{-1}$, $\Delta H = -4.1 \pm 0.2$ kcal/mol, $\Delta S = 12 \pm 0.7$ cal/mol K, and binding site size of four base pairs ($1/n$). The data were fitted starting with different initial values, and they resulted in the above parameters, within our experimental error. Data from multiple titrations were analyzed, and the above values have been the averages over several measurements. Therefore, a single binding site with a moderate affinity accounts for the binding with a strong exothermic reaction, and the use of a more complex model could not be justified. The observed binding constant is more than order of magnitude greater than that of AMAC.[8]

Exothermic binding of a number of probes to DNA was reported earlier,[18] but this is the first example of an anthracene derivative for which the thermodynamic parameters have been measured directly. Encouraged by the data obtained with

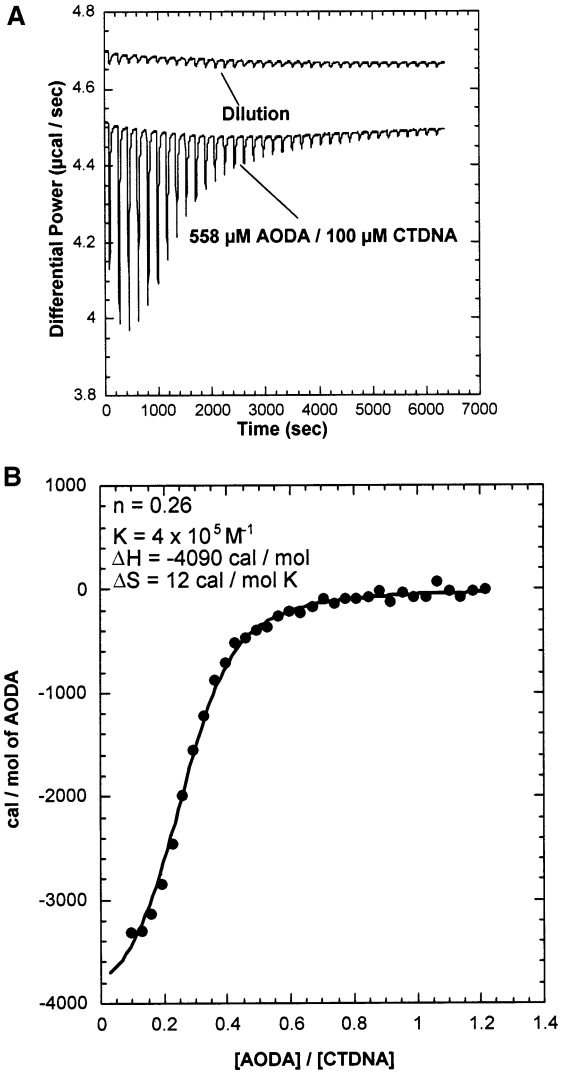

Figure 1. A. Isothermal calorimetric titration curve obtained when a concentrated solution of AODA (558 μM) was added to CT DNA (100 μM), in equal intervals. Top curve shows the heat produced when AODA (558 μM) was added to the buffer, under similar conditions. B. Isothermal calorimetric titration curve obtained when a concentrated solution of AODA (558 μM) was added to CT DNA (100 μM). The solid line indicates the best fit to the data for a single binding site model.

AODA, the binding of AMAC and APAC to CT DNA was tested in ITC studies. Binding of these anthryl probes, in contrast to AODA, indicated that heat release is nearly zero, but their affinity to DNA is not weak.[9] Similarly, a titration of 1,8-octyldiammine·2HCl (512 μM) to CT DNA (100 μM) indicated very weak heat release (data not shown). Therefore, the enthalpy of binding of AODA to CT DNA is far greater than the sum of the heat releases due to the binding of the anthryl nucleus and the octyl side chain. A strong synergistic effect, therefore, is clearly evident for AODA binding to CT DNA.

To further evaluate the details of binding of AODA to CT DNA, spectroscopic studies were carried out, and the calorimetric data are consistent with the absorption and fluorescence data presented below.

Absorption Spectral Studies. The absorption spectra of AODA (17 μM AODA, 5 mM Tris, 50 mM NaCl, pH 7.2) recorded in the presence of increasing concentrations of CT DNA (0−68 μM) are shown in Figure 2. The DNA concentration was increased in small increments, until no further changes are apparent in the absorption spectra, and the spectra have been

TABLE 1: Absorption Peak Positions, Isosbestic Points, Hypochromism, and the Extinction Coefficients (ϵ) for the Free and Bound AODA (5 mM Tris, 50 mM NaCl, pH 7.2). The Excitation Wavelength of the Bound Probe Was 375 nm

	peak positions, nm		extinction coefficient, $M^{-1}\,cm^{-1}$ (nm)			
probe	free	bound	free	bound	isosbestic points	hypochromism (%)
AODA	350, 368, 388	356, 376, 396	4476 (388)	1396 (388)	375, 394	67 (388)
APAC	348, 365, 386	352, 370, 390	7830 (365)	3420 (365)	325, 371, 390	63 (365)
AMAC	348, 365, 385	352, 368, 392	3220 (365)	1276 (365)	362, 367, 388	55 (365)

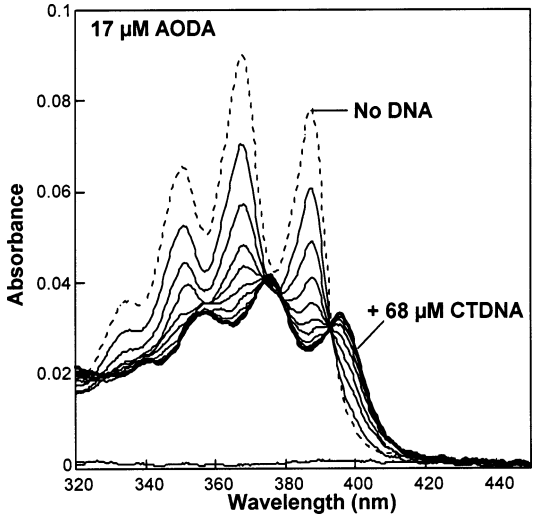

Figure 2. Absorption spectra of AODA recorded in the presence of increasing concentrations of CT DNA (0, 7, 14, 21, 28, 35, 42, 49, 55, 62, and 68 μM). Continuous decrease in the absorbance at the peaks and isosbestic points are evident in the spectra.

CHART 3: Energy Level Diagram for the Electronic Transitions of the Free and Bound Probe

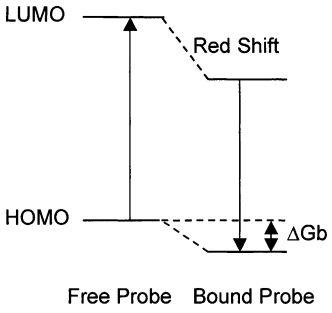

corrected for volume changes during the titration. The spectra indicate a strong decrease in the absorption at the AODA peak positions, considerable broadening of the vibronic bands, and the appearance of a new absorption peak at 396 nm. Isosbestic points (wavelengths where the absorbance is independent of DNA concentration) are observed at 394 and 378 nm. The isosbestic points indicate the presence of two spectroscopically distinct chromophores (free and bound), and this assignment is also consistent with the previous reports on the absorption titrations of anthracene derivatives.[8]

The absorption peak positions of AODA are red-shifted on binding to DNA by 6−8 nm (Table 1), and these are comparable to, or larger than, the red-shifts reported with other anthryl probes.[8] Note that the absorption spectra of AODA/CT DNA mixtures equilibrated rapidly, and these did not show any further changes as a function of time (S1).

The spectral changes in Figure 2 indicate a decrease in the energy gap between the highest occupied molecular orbital (HOMO) and the lowest unoccupied molecular orbital (LUMO) of AODA/CT DNA (Chart 3). In addition to the relative changes in the energies of these states, the exothermic binding of AODA

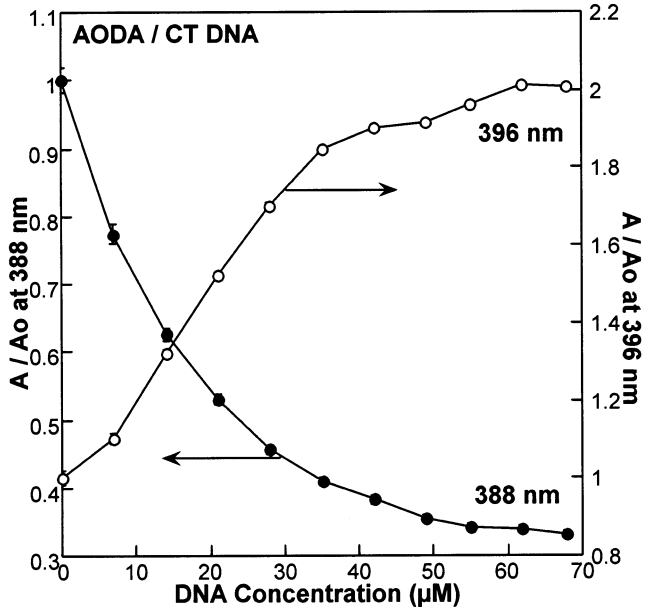

Figure 3. A plot of absorbance of AODA as a function of CT DNA concentration, monitored at 388 nm (decrease) and 396 nm (increase). Error bars shown on each point are too small to be visible.

to DNA, observed by ITC, indicates that the HOMO of the bound probe is stabilized with respect to that of the free probe. The red shift in the absorption spectra, therefore, implies that binding to DNA stabilizes the first excited state of the probe to a greater extent than the ground state. This interaction results in a smaller HOMO−LUMO energy gap.

Since the strength of this interaction between AODA and DNA is inversely proportional to the cube of distance of separation between them,[19] current results suggest that AODA may bind closely to the base pairs, as in the case of intercalative binding.[20] The observed red shifts in the absorption spectra are likely due to excitonic interactions[21] with the electronic states of the base pairs at the intercalation site, but groove binding would not facilitate such interaction. Also note that large red shifts are not observed when the probe solutions were titrated with single stranded DNA or when AODA was added to denatured DNA (data not shown). In addition, when the intercalation of the anthryl chromophore was inhibited by placing a large substitutent at the 9 position of the anthryl ring system, the red shift was very small.[22]

The above absorption spectral data are used further to evaluate the binding. For example, absorbances at 388 and 396 nm are plotted as a function of DNA concentration (Figure 3). The plots show a gradual decrease in the absorbance of the free probe at 388 nm, while there is a concomitant increase in the absorbance at 396 nm due to the bound probe. The data show smooth decreases or increases in the absorption as a function of DNA concentration. This is also consistent with a dominant binding mode.

In addition to the red shifts in the absorption bands reported above, the extinction coefficients of AODA are decreased upon binding to CT DNA by as much as 67% (hypochromism). The

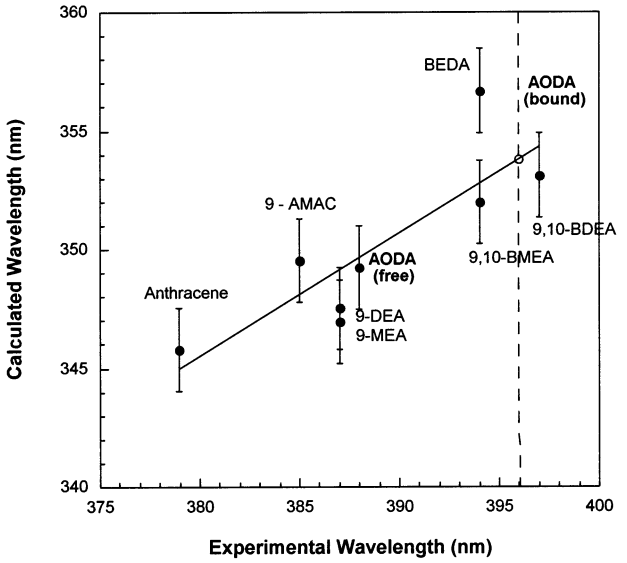

Figure 4. The correlation between the calculated and experimental absorption maxima (0−0′ transitions) for several anthracene derivatives. The error bars on the *Y*-axis are indicative of the widths of the calculated absorbance peaks. The structure of the anthracenes are defined in Supporting Information #2.

decrease is quantified as $(\epsilon_f - \epsilon_b)/100$, and the corresponding data have been collected in Table 1. The extinction coefficients of the bound probe were estimated by extrapolation of the data to high DNA concentrations. The percent hypochromism observed at the corresponding 0−0′ bands (the longest wavelength vibronic peak) is in the order AODA ≈ APAC > AMAC. There has been a strong correlation between intercalation of the anthryl ligand and concomitant red-shifted absorption spectra.[8,9] Intercalation is likely to be the major binding mode but groove binding cannot be completely ruled out.

Computational Modeling of the Absorption Spectra. As a first step toward the computational modeling of binding of AODA to DNA, studies are carried out to compute the electronic properties of AODA. In these studies, the influence of the substitutions at 9 and 10 positions on the electronic absorption spectra of the anthryl ring system is investigated by CAChe. These spectra are used to calculate HOMO−LUMO energy gaps and zero point energies (ZPE). The calculated values of the absorption maxima are plotted as a function of experimentally determined 0−0′ values (Figure 4), and the correlation between the calculated vs the observed values is significant. Note that all calculated values are systematically lower than the observed values, and the calculated values are for the gas phase while the observed values are for the solution phase. In addition, the calculated values correspond to the maxima of the absorption envelope while the measured values are that of the 0−0′ vibronic band, and these differences partially account for the differences in the calculated vs observed values.

The HOMO−LUMO gap follows the order disubstituted anthracenes < monosubstituted anthracenes < anthracene. Plotted on this graph is the observed 0−0′ band of the AODA/CT DNA (vertical line), and this line falls in the region of the energy gap for a disubstituted anthracene. Binding to DNA, therefore, causes electronic effects that are similar to additional substitution on the anthryl ring system. This scenario was also noted with other monosubstituted anthracene ligands.

Encouraged by these results, the above studies were extended to evaluate the vibrational energy gaps in the ground and first excited electronic state of AODA. The frequencies of 165 virbrational modes of AODA, in both the ground and the excited

TABLE 2: Calculated and Experimental Values for the Vibronic Transitions of AODA (0−0′, 0−1′, and 0−2′) and Related Parameters

ΔE^a	calculated, cm^{-1} (nm)	experimental, cm^{-1} (nm)
0−0′	29070 (344)	25773 (388)
0−1′	30462 (328)	27174 (368)
0−2′	31854 (314)	28571 (350)
0′-1′	1392	1401
1′-2′	1392	1398
ZPE	619	613
ZPE*	696	700
HOMO-LUMO	28993 (345)	25686 (388)

[a] * First excited-state values.

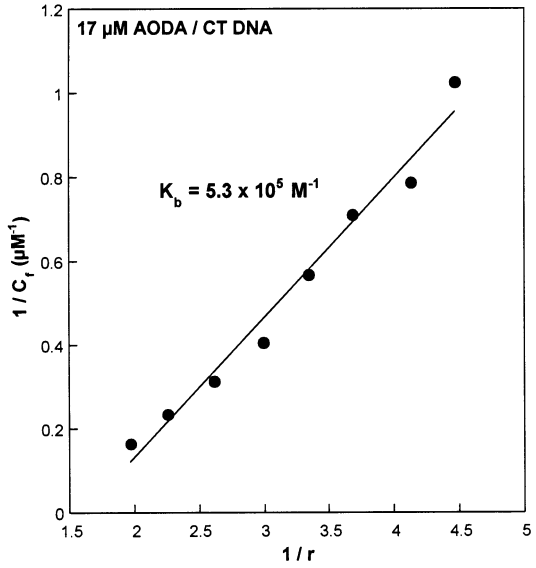

Figure 5. Scatchard plot for the binding of AODA to CT DNA (5 mM Tris, 50 mM NaCl, pH 7.2), and the data have been fitted to the Scatchard equation (solid line).

state, as well as the zero point energies (ZPE), were calculated using MOPAC with PM3 parameters. The vibrational frequencies were then used to construct the IR spectra of the ground and first excited electronic states of AODA (S3). The calculated and the experimental values are listed in Table 2, and the ZPE showed excellent correlation with the experimental values. Calculated vibronic bands deviated from the observed values, discussed above, but the 0′−1′ and 1′−2′ energy gaps matched well. Note that 0′−1′ and 1′−2′ energies correspond to the spacings of the vibronic bands in the absorption spectrum while the 0−1 and 1−2 correspond to those in the fluorescence spectra. The calculations overestimate the HOMO−LUMO gap but estimate the vibrational spacings more accurately. Future studies will focus on modeling the influence of intercalation on these energy gaps.

Binding Plots. Scatchard plots were constructed from the extinction coefficients of the free and bound AODA, the concentrations of the bound and free AODA, and the binding density (*r*) (Figure 5). Linear least-squares fits to the data (solid line) indicated the corresponding binding parameters (Table 3). The average binding constant estimated from these data ($5.3 \pm 1 \times 10^5$ M^{-1}) is in good agreement with the calorimetric data presented above ($4.0 \pm 0.4 \times 10^5$ M^{-1}). The binding constant of AODA is considerably higher (∼35 times) than the values reported for APAC and AMAC at the same ionic strength and pH. This large increase in K_b is a direct indication of the strong role of the side chain in promoting AODA interaction with DNA.

TABLE 3: Comparison of the Binding Constants of AODA, APAC, and AMAC (CT DNA)

		fluorescence, λ_{max} (nm)		Stokes shift (cm^{-1})	
probe	K_b, M^{-1}	free probe	bound probe	free probe	bound probe
AODA	5.3×10^5 (396)	394, 414, 440	402, 424, 450	392	377
APAC	$1.4 \pm 0.1 \times 10^4$ (365)	390, 412, 437	391, 413, 438	266	66
AMAC	$1.5 \pm 0.5 \times 10^4$ (365)	392, 412, 438	395, 413, 438	464	194

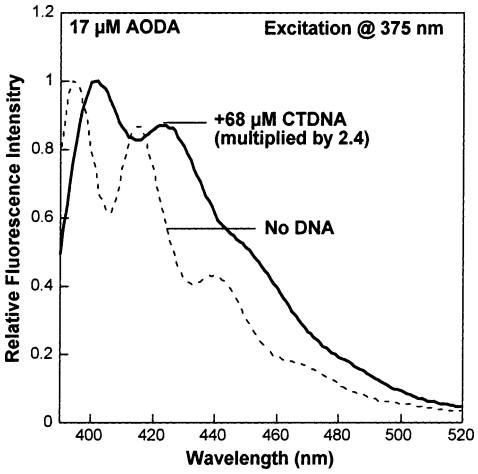

Figure 6. Fluorescence spectra of AODA recorded in the absence and presence of CT DNA.

Fluorescence Studies. Fluorescence spectra of AODA provided additional opportunities to examine the details of the interaction of anthryl probes with DNA. The fluorescence spectra of AODA were recorded in the presence of increasing concentrations of CT DNA, and the data at one concentration have been shown in Figure 6. The probe/DNA samples were excited at the isosbestic point (375 nm) so that absorbance of the sample was independent of DNA concentration. The fluorescence spectra indicate red shifts of the peak positions, decreases in intensity, and broadening of the vibronic bands. The peak wavelengths shifted from 394, 414, and 440 nm (free probe) to 402, 424, and 450 nm (bound), respectively. These shifts are consistent with the red shifts observed in the absorption spectra shown above, and this is also consistent with the decrease in the HOMO−LUMO energy gap. Accurate measurement of these shifts for the bound AODA, however, is complicated due to the strong quenching of fluorescence by DNA ($K_{sv} = 2.0 \times 10^4$ M^{-1}). Such strong quenching of anthryl fluorescence by DNA was also observed with other anthryl probes.[9]

Circular Dichroism (CD) Studies. Although AODA is not chiral, its association with the right-handed DNA helix is expected to result in strong CD spectra in the absorption regions of the probe, away from the DNA absorption bands. Furthermore, induced CD spectra of the intercalated and groove bound chromophores are expected to be different.[23] By recording the CD spectra at increasing ratios of AODA to DNA concentrations, the relative populations of these binding modes can be ascertained. The CD spectra of AODA recorded at increasing AODA:DNA ratios are presented in Figure 7. At low loadings (ratio of 1:4), strong, positive, induced CD bands appeared at 345, 365, 376, and 396 nm, and only some of these correspond to the absorption peak positions of the bound probe (356, 376, and 396 nm, Figure 2). At low loading, the number of binding sites is adequate for the intercalation of all the probe molecules, and at higher loadings groove binding or outside stacking may also occur. Due to the lack of a chiral center in AODA, the free probe cannot contribute to the CD spectrum. The positive CD bands are assigned to the intercalated chromophore where

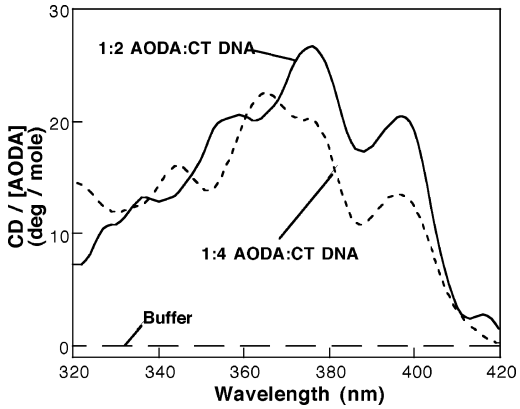

Figure 7. The induced circular dichroism spectra of AODA (150 μM) recorded at low and high ratios of AODA: CT DNA concentrations. Only some peaks match between the two spectra.

CHART 4: Energy Level Diagram for the Energy Transfer from DNA to Bound AODA

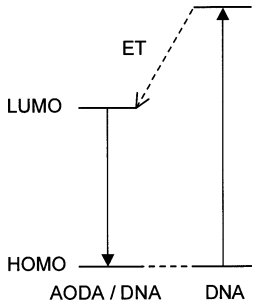

the long axis of the anthryl moiety is aligned perpendicular to the long axis of the DNA base pairs.[23,24]

At high loadings (1:2 ratio) of AODA:DNA, not all the probe molecules can be accommodated by intercalation alone. Note that the binding site size was four base pairs (ITC data) and larger than what is expected from the neighbor exclusion principle. Thus, both groove binding and intercalation are expected to contribute to the CD spectra. Outside stacking is another binding mode that can contribute to these spectra. Regardless of the binding modes, the CD spectra clearly indicate a strong electronic interaction between the AODA chromophore and the DNA bases.

Sensitized Fluorescence. To further investigate the binding of AODA to CTDNA, energy transfer from DNA bases to the probe was examined in fluorescence studies. The emission spectra of the DNA bases overlap with the absorption spectra of the anthryl probes, and energy transfer from the DNA excited states to AODA is expected to be exothermic. Earlier studies from this laboratory indicated that excited states of the DNA bases can transfer energy to the anthryl probe (Chart 4), and energy transfer was efficient from AT binding sites.[25] Energy transfer was inhibited when the DNA helix was denatured, and only weak energy transfer was noted with probes where intercalation was inhibited by placing large substituents at the 9 and 10 positions of the anthryl ring system.[26] Energy transfer from CT DNA to AODA was monitored, in two separate

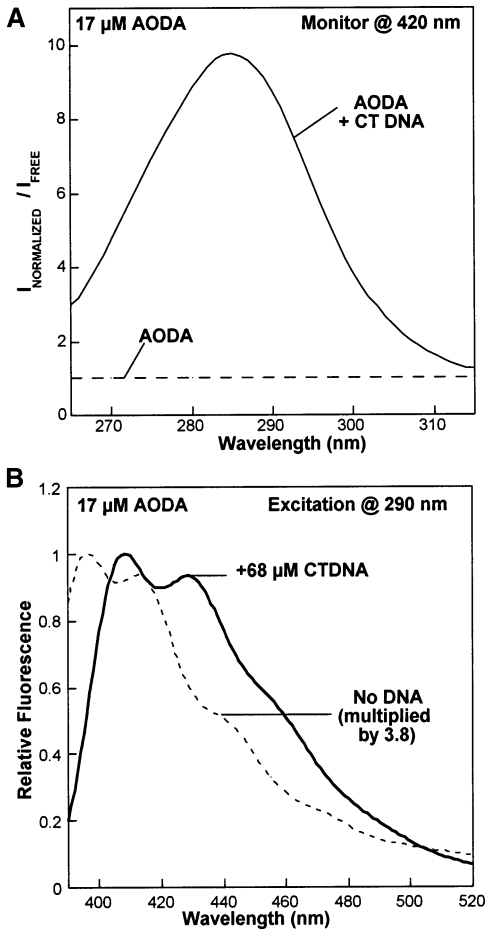

Figure 8. A. Excitation spectra of AODA bound to CT DNA (68 μM). The ratio of fluorescence intensity in the presence of DNA to that in the absence of DNA is shown. Values greater than one on the *Y*-axis indicate sensitization of fluorescence by the DNA bases. B. Fluorescence spectra (290 nm excitation) of AODA recorded in the absence and presence of CT DNA. Strong increase in the intensity (3.8×) and a red-shift are evident in the spectra. The spectra have been normalized by multiplying with a suitable value.

experiments, by recording excitation spectra and sensitized fluorescence spectra.

The excitation spectrum of AODA/CT DNA was recorded in the 250−300 nm region by monitoring AODA emission at 420 nm (Figure 8A). CT DNA did not have detectable emission at 420 nm, and absorbance of AODA in the 250−300 nm is minimal. To account for any direct emission from AODA, the ratio of the excitation spectrum of AODA in the presence of CT DNA to that in the absence of CT DNA was shown in Figure 8A. If there is no energy transfer, then one may anticipate a flat baseline with an intercept of one. On the contrary, a new intense band at ∼285 nm is detected, and this peak corresponds to the absorption bands of DNA bases.[27] The singlet energies of all the bases are much greater than that of AODA, and exothermic energy transfer to AODA is expected. When the DNA helix was denatured, by raising the temperature (>80 °C), the sensitized emission was abolished.

To confirm that the sensitized emission detected at 420 nm is indeed from AODA, the emission spectra of AODA/CT DNA mixtures (290 nm excitation) were recorded (Figure 8B). The sensitized fluorescence spectra of AODA are very similar to that of direct emission spectra (Figure 6), but the peak positions are further red shifted by ∼5 nm. However, the sensitized emission was much more intense than direct emission from AODA/CT DNA by a factor of ∼10. The excitation and the fluorescence spectra provided a direct evidence for energy transfer from the DNA bases to AODA.

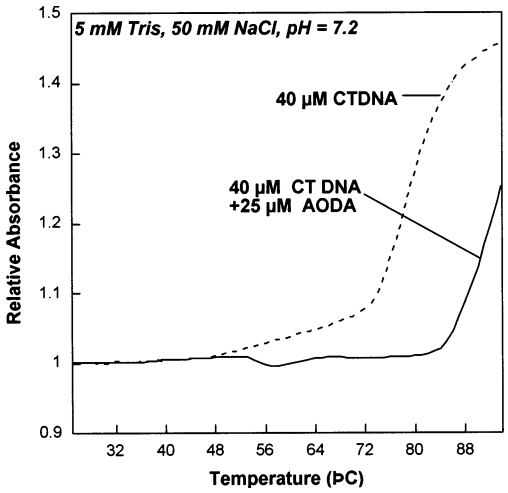

Figure 9. Helix melting curves of CT DNA in the presence (solid line) and in the absence (dashed line) of AODA. The clear increase of T_m by AODA is evident from these data.

Note that when excited at 375 nm, CT DNA quenched direct emission of AODA but excitation at 290 nm resulted in intense, sensitized emission. This apparent discrepancy of CT DNA functioning both as a sensitizer and quencher can be resolved. Previous studies with anthracene derivatives showed that sensitization by DNA is most efficient when bound to AT sites, and quenching was most effective at GC sites.[9] Therefore, excitation at 375 nm permits probing the quenching behavior of DNA, and no sensitization can occur, under these conditions. Excitation at 296 nm, on the other hand, results in energy transfer from the AT bases to the chromophore bound at these sites and intense emission is observed. AT sequences did not quench anthryl emission to a significant extent, and sensitized fluorescence is likely from AODA bound to AT sites. Also note that the sensitized fluorescence spectra of AODA/CT DNA are red-shifted by ∼6 nm, when compared to direct emission of AODA/CT DNA. This also clearly indicated that only a fraction of the bound chromophores are sensitized by DNA. It is possible that energy is transferred efficiently to the intercalated AODA at AT sites.

Helix Melting Studies. Binding of the ligand to the DNA may stabilize or destabilize the helix, and these changes are monitored in helix melting studies. Intercalative binding of the anthracene derivatives is expected to enhance the thermodynamic stability of the double helix and raise the helix melting temperature (T_m),[28] although some groove binders also raise T_m. Regardless of the binding mode, this thermodynamic parameter is a characteristic of the type of interaction between the ligand and the helix. Helix melting was monitored by recording the CT DNA absorbance at 260 nm as a function of temperature, and when the double helix dissociates into single-stranded DNA, the absorbance is increased substantially. The midpoint of the transition represents the temperature where the concentration of the double helix is reduced to one-half. Binding of many anthryl derivatives improved the helix stability to a large extent, and the helix melting curves of CT DNA with and without AODA (5 mM Tris, 50 mM NaCl, pH 7.2) are shown in Figure 9.

The ratio of absorbance of the sample at room temperature to the absorbance at elevated temperature was plotted as a function of temperature, so that the plots originate at the same *Y*-value. As the temperature is increased, the ratio remained

nearly constant, and then it increased rapidly around the T_m of the sample. For example, CT DNA indicated a T_m of 78 °C in the absence of AODA, and this value was substantially increased to >90 °C, in the presence of AODA. In fact, the helix melting is not completed even at ~92 °C which indicated that the helix is stabilized by AODA to a large extent. The temperature of the sample could not be increased further due to losses by evaporation/boiling of the buffer. Based on the spectral data, as well as the increased helix melting temperatures, intercalation of AODA into the helix is very likely. The T_m of AODA/CT DNA did not depend on the rate at which the samples were heated or when the samples have been preheated at 65 °C for 0.5 h (data not shown).

Ionic Strength Studies. Binding of the ligands to DNA is expected to decrease with increased ionic strength. However, groove binding and intercalative binding are expected to differ in terms of their dependence on ionic strength.[29] Increased ionic strength screens the phosphate−phosphate repulsion, and the helix shrinks. Such helix collapse is expected to adversely affect intercalation and groove binding. At low ionic strengths, on the other hand, intercalation may dominate due to larger phosphate−phosphate distances and wider grooves. Such groove widening may preclude a snug fit of the ligand. Therefore, the relative energetics of groove binding and intercalation may change as a function of ionic strength. For anthracene probes such as AODA where steric factors are not important, intercalation may be favored at low ionic strengths and groove binding may persist at high ionic strengths. These expectations are tested with AODA by examining the effect of ionic strength in absorption, fluorescence, and energy transfer experiments where the ionic strength is increased by the addition of appropriate volumes of concentrated NaCl solutions.

Absorption studies were the most revealing (S4). At low ionic strengths (10, 20, and 38 mM NaCl), the absorption spectrum of the probe/DNA mixtures (ratio of concentrations of the probe to DNA is 1:4) is nearly identical to that recorded at 50 mM NaCl, and the new red shifted absorption peak at 396 nm, as well as extensive hypochromism, is clearly evident. The data have been corrected for volume changes, and the absorption spectra of the free AODA did not show any dependence on ionic strength. As the ionic strength is raised further by the addition of NaCl solution, the strength of the 396 nm peak decreased rapidly, and peaks corresponding to the free probe began to emerge. At 285 mM NaCl, the absorbance of AODA/CTDNA @ 388 nm is still much less than that of the free AODA, and the peak at 396 nm has nearly disappeared. It is very likely that the absorption spectrum at this ionic strength (285 mM) corresponds to the sum of the spectra due to the free ligand, intercalated ligand, and groove-bound ligand.

For example, the observed spectrum did not match with that of the free probe after attenuation by a suitable factor, nor did this spectrum correspond to a sum of the spectra of the free and the bound probe. Adjusting the proportions of the components did not improve the situation. Therefore, a third component is essential to explain the spectra, which is likely to be the groove-bound ligand. Unshifted absorption spectra were noted when intercalation of the anthryl ring system was inhibited due to large substituents at the 9 position of the anthryl ring system, and the groove-bound spectrum is likely to show little or no red shifts.[26,22]

In a similar manner, the fluorescence spectra of AODA/CTDNA recorded at increasing ionic strengths are shown in Supporting Information (S5). Increasing ionic strength resulted in considerable blue shifts in the fluorescence maxima, and the spectra at high ionic strengths resemble the spectra of the free probe. Note that the spectra are normalized, NaCl does not quench AODA emission, and even at high ionic strengths there is considerable reduction in intensity when compared to that of free AODA. This is consistent with the absorption data presented above. In a similar manner, the excitation spectra recorded in the 250−320 nm region (420 nm monitoring, S6) also show that sensitized emission is diminished drastically at high ionic strengths.

These various lines of ionic strength studies show that (a) binding of AODA to CT DNA is reversible to a large extent, (b) binding is dependent on the ionic strength of the medium, and (c) at high ionic strengths one of the binding modes is diminished considerably but another binding mode persists. If there are two distinct binding modes for AODA, they are resolvable in ionic strength studies, and these will be the focus of future studies.

Conclusions

Binding of AODA to CT DNA is exothermic with a substantial increase in entropy. A large share of the thermodynamic changes are contributed by the octyl side chain, and this provides a simple strategy to enhance the overall binding affinity. Occasionally, even minor structural variations of the substituents can have pronounced influence on the binding of an intercalator.[30−35] Calorimetric studies, presented here, clearly indicate a strong synergistic effect of the side chain and the anthryl nucleus. These imply that AODA invokes new interactions with DNA that are not available with AMAC or 1,8-octyldiamine. This insight will be useful in future designs of DNA probes. Spectroscopic studies complement the thermodynamic studies, and binding involves strong electronic interactions with the DNA bases. These interactions in turn result in strong hypochromism, red shifts, and reduced fluorescence intensities. The large increase in the T_m, strong hypochromism, induced circular dichroism, and energy transfer from the DNA bases to the anthryl chromophore all strongly indicate intercalative binding as one of the major binding components. Future studies will be designed test these conclusions.

Acknowledgment. Financial support from the National Science Foundation is gratefully acknowledged (DMR-0300631), and we thank M. R. Duff for experimental assistance with the ITC.

Supporting Information Available: Experimental details. This material is available free of charge via the Internet at http://pubs.acs.org.

References and Notes

(1) Neidle, S., Waring, M., Eds.; *Molecular Aspects of Anticancer Drug−DNA Interactions*; CRC: Boca Raton, 1993; Vols. 1 and 2. D'incalci, M.; Sessa, C. *Expert Opin. Invest. Drugs* **1997**, *6*, 875.

(2) Frei, E.; Luce, J. K.; Loo, T. L. *Cancer Chemother. Rep., Part 1* **1971**, *55*, 91.

(3) Wilson, W. L.; Weiss, A. J.; Andrews, N. C. *Cancer Chemother. Rep., Part 1* **1971**, *55*, 525.

(4) Remers, W. A.; Wunz, T. P.; Dorr, R. T.; Alberts, D. S.; Tunget, C. L.; Einspahr, J.; Milton, S. *J. Med. Chem.* **1987**, *30*, 1313−1321.

(5) Remers, W. A.; Dorr, R. T.; Alberts, D. S.; Iyengar, B. S.; Solyom, A. M.; Krutzsch, M. *J. Med. Chem.* **1997**, *40*, 3734−3738.

(6) Wang, L.; Price, H. L.; Juusola, J.; Kline, M.; Phanstiel, O., IV. *J. Med. Chem.* **2001**, *44*, 3682−3691.

(7) Wilson, W. D.; Wang, Y. H.; Kusuma, S.; Chandrasekharan, S.; Yang, N. C.; Boykin, D. W. *J. Am. Chem. Soc.* **1985**, *107*, 4989−4995.

(8) Kumar, C. V.; Asuncion, E. H. *J. Am. Chem. Soc.* **1993**, *115*, 8547−8553.

(9) Kumar, C. V.; Asuncion, E. H.; Tan, W. B. *Tetrahedron* **2000**, *56*, 7027−7040.
(10) Wilson, W. D.; Tanious, F. A.; Watson, R. A.; Barton, H. J.; Strekowska, A.; Harden, D. B.; Strekowski, L. *Biochemistry* **1989**, *28*, 1984.
(11) Lerman, L. S. *J. Mol. Biol.* **1961**, *3*, 18.
(12) Tabor, C. W.; Tabor, H. *Annu. Rev. Biochem.* **1984**, *53*, 749.
(13) Maniatis, T.; Fritsch, E. F.; Sambrook, *J. Molecular Cloning: a Laboratory Manual*; Cold Spring Harbor Laboratory: New York; p 458.
(14) Breslauer, K. J.; Freire, E.; Straume, M. *Methods Enzymol.* **1992**, *211*, 533; Sturtevant, J. M. *Annu. Rev. Biochem.* **1987**, *38*, 463−88.
(15) Barton, J. K.; Goldberg, J. M.; Kumar, C. V.; Turro, N. J. *J. Am. Chem. Soc.* **1986**, *108*, 2081. Baguley, B. C.; Falkenhaug, E. M. *Nucleic Acids Res.* **1978**, *5*, 161.
(16) McGhee, J. D.; von Hippel, P. H. *J. Mol. Biol.* **1974**, *86*, 469.
(17) Chaires, J. B. *Biopolymers* **1997**, *44*, 201−215.
(18) Ren, J.; Jenkins, T. C.; Chaires, J. B. *Biochemistry* **2000**, *39*, 8439−47.
(19) Cantor, C.; Schimmel, P. R. *Biophysical Chemistry*, W. H. Freeman: San Francisco, 1980; Vol. *2*, p 398.
(20) Long, E. C.; Barton, J. K. *Acc. Chem. Res.* **1990**, *23*, 271; Dougherty, G.; Prigram, W. J. *Crit. Rev. Biochem.* **1982**, *12*, 103; Berman, H. M.; Young, P. R. *Annu. Rev. Biophys. Bioeng.* **1981**, *10*, 87.
(21) Kasha, M. *Radiation. Res.* **1963**, *20*, 55.
(22) Becker, H.-C.; Norden, B. *J. Am. Chem. Soc.* **1999**, *121*, 11947.
(23) Norden, B.; Kurucsev, T. *J. Mol. Recognit.* **1994**, *7*, 141−55.
(24) Asuncion, E. H., Ph.D. Thesis, University of Connecticut, 1994.
(25) Kumar, C. V.; Asuncion, E. H. *J. Am. Chem. Soc.* **1992**, *115*, 8547.
(26) Tan, W. B. Ph.D. Thesis, University of Connecticut, 2000.
(27) Amundsen, L. H.; Nelson, L. S. *J. Am. Chem. Soc.* **1951**, *73*, 242.
(28) Berman, H. M.; Young, P. R. *Annu. Rev. Biophys. Bioeng.* **1981**, *10*, 87. Wilson, W. D.; Wang Y. H.; Kusuma, S.; Chandrasekaran, S.; Yang, N. C.; Boykin, D. W. *J. Am. Chem. Soc.* **1985**, *107*, 4989; Wunz, T. P.; Craven, M. T.; Karol, M. D.; Hill, G. C.; Remers, W. A. *J. Med. Chem.* **1990**, *33*, 1549; Wunz, T. P.; Dorr, R. T.; Alberts, D. S.; Tunget, C. L.; Einspahr, J.; Milton, S.; Remers, W. A. *J. Med. Chem.* **1987**, *30*, 1313.
(29) Chirvony, V. S.; Galievsky, V. A.; Terekhov, S. N.; Dzhagarov, B. M.; Ermolenkov, V. V.; Turpin, P. Y. *Biospectroscopy* **1999**, *5*, 302−312.
(30) Atwell, G. J.; Baguley, B. C.; Denny, W. A. *J. Med. Chem.* **1988**, *31*, 774−779.
(31) Atwell, G. J.; Bos, C. D.; Baguley, B. C.; Denny, W. A. *J. Med. Chem.* **1988**, *31*, 1048−1052.
(32) Palmer, B. D.; Rewcastle, G. W.; Atwell, G. J.; Baguley, B. C.; Denny, W. A. *J. Med. Chem.* **1988**, *31*, 707−712.
(33) Rewcastle, G. W.; Baguley, B. C.; Denny, W. A. *J. Med. Chem.* **1987**, *30*, 843−851.
(34) Atwell, G. J.; Rewcastle, G. W.; Baguley, B. C.; Denny, W. A. *J. Med. Chem.* **1987**, *30*, 664−669.
(35) Atwell, G. J.; Cain, B. F.; Baguley, B. C.; Finlay, G. J.; Denny, W. A. *J. Med. Chem.* **1984**, *27*, 1481−1485.